LAWRENCE
LIVERMORE
NATIONAL
LABORATORY

UCRL-JRNL-217296

Bacillus atrophaeus Outer Spore Coat Assembly and Ultrastructure

M. Plomp, T. J. Leighton, K. E. Wheeler, M. E. Pitesky, A. J. Malkin

November 23, 2005

Langmuir

Updated October 14, 2003

For Table of Contents Only

Bacillus atrophaeus Outer Spore Coat Assembly and Ultrastructure.

Marco Plomp, Terrance J. Leighton, Katherine E. Wheeler, Maurice E. Pitesky and Alexander J. Malkin

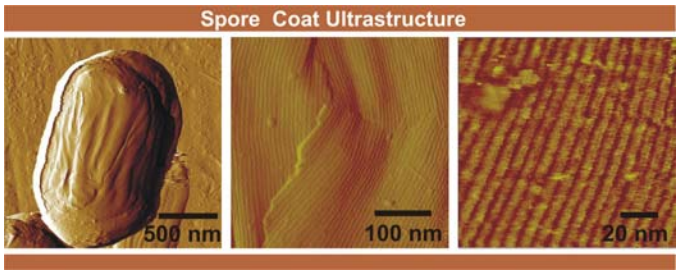

Bacillus atrophaeus Outer Spore Coat Assembly and Ultrastructure

Marco Plomp[1], Terrance J. Leighton[2], Katherine E. Wheeler[2], Maurice E. Pitesky[1] and Alexander J. Malkin[1,*]

[1]*BioSecurity & NanoSciences Laboratory, Department of Chemistry and Materials Science, Lawrence Livermore National Laboratory,L-234, 7000 East Ave, Livermore, CA 94551,* [2]*Children's Hospital Oakland Research Institute, 5700 Martin Luther King Way, Oakland, CA 94609*

*Corresponding author: Mailing address: BioSecurity and NanoSciences Laboratory, Department of Chemistry and Materials Science, Lawrence Livermore National Laboratory, L-234, Livermore CA 94551. Phone: (925) 423-7817; FAX: (925) 422-2041. E-mail: malkin1@llnl.gov

`

ABSTRACT

Our previous atomic force microscopy (AFM) studies successfully visualized native *Bacillus atrophaeus* spore coat ultrastructure and surface morphology. We have shown that the outer spore coat surface is formed by a crystalline array of ~11 nm thick rodlets, having a periodicity of ~8 nm. We present here further AFM ultrastructural investigations of air-dried and fully hydrated spore surface architecture. In the rodlet layer, planar and point defects, as well as domain boundaries, similar to those described for inorganic and macromolecular crystals, were identified. For several *Bacillus* species, rodlet structure assembly and architectural variation appear to be a consequence of species-specific nucleation and crystallization mechanisms that regulate the formation of the outer spore coat. We propose a unifying mechanism for nucleation and self-assembly of this crystalline layer on the outer spore coat surface.

INTRODUCTION

Nanometer scale characterization of native bacterial spore surface structures is essential to elucidating mechanisms of pathogenesis, immune response, hydrophobicity, adhesion, dispersal and response to environmental cues. The structure of fungal and bacterial spores has been the subject of many electron microscopy (EM) studies utilizing freeze-etching, negative staining and thin sectioning methods.[1–3] These studies have shown the presence of substructures within the spore coat, which include rodlet and pitted layers formed by crystalline arrays of coat macromolecules and parasporal structures found exterior to the spore coat and exosporium. A major limitation of conventional EM techniques is that they are not able to provide images of specimens under native physiological conditions. Traditional EM sample preparation can require fixation, embedding and staining regimes that may alter native structures. For example, cryo-EM analysis,[4] which permits visualization of large macromolecular assemblies in their unfixed state, demonstrated that a number of structural features prominent in conventional EM images of vaccinia virus were artifacts resulting from dehydration and non-isotropic collapse of virions during sample preparation.[5]

The development and application of high-resolution techniques that can interrogate native microbial structures are paramount for understanding pathogen architecture. One such emerging technique is atomic force microscopy (AFM),[6] which allows direct visualization of macromolecular assemblies *in vitro* at near-molecular resolution. Cryo-EM-based image reconstruction analysis requires high particle symmetry,[4] while AFM can readily produce high-resolution images of polymorphic and non-uniform microbial populations.

There has been continuous progress in the quality of AFM imaging of biological samples. In particular, structure and conformational changes of membrane proteins,[7–10] DNA, DNA-protein complexes,[11–13] and macromolecular crystallization[14–18] have been intensively studied. AFM has also been utilized for structural studies of various pathogens, including viruses,[19–23] bacteria and microbial spores.[24–26] These studies have demonstrated that AFM has the capacity to provide direct, high-resolution structural, functional and topological characterization of biological surfaces.

Application of AFM to studies of fungal spore surfaces revealed high-resolution spore coat structures and allowed mapping of adhesion interactions on the spore surface.[26,27] The surface morphology and properties of bacterial spores has been studied by AFM;[28–30] however, high-resolution structural analysis of bacterial spore surfaces has not been achieved. Recently, we have utilized AFM[31,32] to visualize the high-resolution native structures of bacterial endospores including the exosporium and crystalline coat layers of several species of *Bacillus* spores (*B. atrophaeus*, *B. cereus* and *B. thuringiensis*). We have demonstrated that spore coat structures are species-dependent. A crystalline hexagonal honeycomb structure was found in *B. thuringiensis* and *B. cereus* spore coats, while crystalline rodlet layers were present in *B. atrophaeus* and *B. cereus* spore coats. We further suggested that the observed species-dependent structural motifs could be a consequence of crystallization conditions, which may regulate the assembly of the outer spore coat.[31,32]

B. atrophaeus spores have been used as a biological indicator for decontamination and sterilization processes,[33–35] bioaerosol detection development[36–38] and as an environmental biotracer.[39] Despite the reliance on *B. atrophaeus* for a wide range of

biological applications, very little is known about its spore surface and coat structure or the effects of growth and environmental manipulations on spore dimensionality.

Here we further investigate the spore coat assembly and architecture of *B. atrophaeus* spores. In this study we utilize AFM methodologies to examine the detailed high-resolution architecture of air-dried and fully hydrated *B. atrophaeus* spore surfaces. Comprehensive studies of several hundred individual spores allowed us to assess the structural variations of the outer spore coat crystalline rodlet layer within spore populations and to derive a model for its assembly. We also describe how AFM imaging conditions and parameters affect the resolution of bacterial spore surface architecture.

MATERIALS AND METHODS

Spore Preparation and Purification. *B. atrophaeus* (ATCC 9372) spores used in this study were produced using two methods. Method A: Cells were grown to mid-log phase in Nutrient Broth and then aliquoted at a 1:25 dilution into ¼ Tryptone Yeast Extract (1/4 TY).[40] Method B: *B. atrophaeus* spores were prepared and purified as described.[41,42] Spore preparations were stored at 4°C.

Atomic force microscopy. Droplets of *B. atrophaeus* suspension (0.5–3 µl) were deposited directly onto a substrate and were allowed ~10 minutes to settle, after which the sample substrate was rinsed with double distilled water. For imaging in air, the samples were dried and imaged. For imaging of air-dried spore samples and fully hydrated spore samples, freshly cleaved mica and polycoated vinyl plastic were utilized as a substrate.

Images were collected using Digital Instruments Multimode Nanoscope IIIa and IV atomic force microscopes (Veeco, Santa Barbara, CA) operated in tapping mode. In

tapping mode virtually no lateral forces are applied to the sample during imaging,[43] which makes it the preferred approach to probe biological structures at high resolution. Since spore adhesion to the substrate is typically weaker in liquid compared to air-dried spores, application of tapping mode is particularly important for the former case to prevent removal of spores by the AFM tip.

Tapping amplitude, phase and height images were collected simultaneously. Height images were primarily used for quantitative measurements, while amplitude and phase images were predominantly used for presentation. Etched silicon tips (force constants of ~40 N/m and resonance frequencies of ~300 kHz) and oxide-sharpened silicon nitride tips (force constants of approximately 0.1 N/m and resonance frequencies of ~9 kHz) were purchased from Veeco and employed for imaging in air and fluid, respectively.

RESULTS AND DISCUSSION

Surface morphology of air-dried spores: **Optimization of imaging parameters for high-resolution visualization of the spore coat**. AFM images of air-dried spore preparation from *B. atrophaeus* adsorbed on mica are shown in Figure 1a–c. The most prominent surface features seen on air-dried spores were ridges (indicated with arrows in Figure 1b), which typically extended along the long axis. The thickness of these ridges varied from 30–60 nm. Similar ridges were previously reported by electron microscopy[1,2] and AFM studies of various species of bacterial spores.[30–32]

The dynamic ability of the coat to fold and unfold concomitant with changes in spore size was suggested recently[30,44] based on measurements of *B. thuringiensis* spore dimensions induced by humidity transients.[45] The direct visualization of responses of a

single *B. atrophaeus* spore to dehydration transients has demonstrated that the spore core and/or cortex contract and that the spore coat accommodates this decrease in internal volume by surface folding and ridge formation.[31]

High-magnification imaging of bacterial spore surfaces often fails to reveal the molecular structure of the spore coat. Low-resolution AFM images of several *Bacillus* species spores have been reported.[28-30] It was suggested[30] that the absence of high-resolution spore surface structures may be due either to the desiccated state of the bacterial spores examined or the removal of the surface layer during sample processing.

We have reported previously[31,32] high resolution structures of the outer spore coat of *B. atrophaeus*, *B. thuringiensis* and *B. cereus* spores. These studies demonstrated that the outer surface of the spore coat is formed by species-specific arrays of macromolecules forming either rodlet or honeycomb crystalline structures. Thus, successful high-resolution AFM imaging of both air-dried and fully hydrated bacterial spores is possible, though it depends strongly on the imaging conditions and parameters.

As seen in Fig. 1c, large areas of regular rodlet structures (indicated with an arrow) were visible even with a relatively large scan size. These rodlets were up to 1 μm in length, 10–11 nm thick and had a periodicity of ~8 nm. Similar rodlet structures were seen previously in freeze-etching EM studies of several fungal and bacterial spores.[1–3] AFM studies of the surface morphology of *Phanerochaete chrysosporium* fungal spores[27] and *Bacillus* spores[31,32] confirmed the existence of rodlet structures.

Possible explanations for previous difficulties in the AFM imaging of spore surface ultrastructure are two-fold. First, surfaces of air-dried bacterial spores appear to be heterogeneous, with partial coverage by contaminating debris which may either attach

to the surface during spore preparation or sediment onto the spores during the drying process. We found that a combination of rigorous spore purification and extensive yet gentle rinsing following attachment of spores to the substrate markedly reduced spore-associated debris. Secondly, the AFM imaging parameters and tip sharpness are pivotal, even in a case where the spore coat surface is not obscured by debris. Images of soft biological samples are typically recorded utilizing light tapping, with A_{sp}/A_o ~0.8. Here A_{sp} and A_o are the free and the set-point amplitudes, respectively, of an oscillating AFM probe. With these imaging conditions, tip-sample contact is minimal, and the oscillating AFM probe makes only brief contact with the sample surface in each oscillation cycle. Tip-sample force interactions can be increased by either increasing the amplitude A_o or decreasing the set-point amplitude A_{sp},[46] both of which result in an increase of energy dissipated in the scanning area during the tip-sample contact. AFM studies of polymers have demonstrated that high-resolution visualization of heterogeneous multi-component compounds could not be achieved with light tapping due to minimal tip-sample interactions.[43] However, resolution was greatly enhanced during imaging of polymer samples by hard tapping applying a considerably decreased A_{sp}/A_o ratio.[43,47]

Tip-sample force interactions are dependent on the sharpness and overall shape of the AFM probe. Commercial AFM probes can be dull or can become dull during imaging due to wear or contamination with debris. In these cases a significant decrease in the A_{sp}/A_o ratio is required. Typically, ratios of A_{sp}/A_o ~0.4–0.5 were sufficient for successful high-resolution visualization of spore coat ultrastructure, while, for duller probes, ratios of 0.1–0.2 were required.

Imaging of the spore surface with a dull probe is illustrated in Figure 2 where moderate tapping ($A_{sp}/A_o = 0.7$) resulted in a featureless image of the surface (Figure 2a). When the A_{sp}/A_o ratio was decreased to 0.4, high-resolution structures emerged (Figure 2b). Imaging by hard tapping ($A_{sp}/A_o = 0.2$) revealed the complete nanoscale structure of the spore coat surface, as illustrated in Figure 2c.

In the case of a dull probe, the requirement for harder tapping may be a consequence of its geometry. Sharp micro-protrusions could form on the surface of AFM probes during the manufacturing process. In the case of a dull probe, harder tapping may be required to allow one of the sharp micro-protrusions to contact the sample and provide a detailed image of the surface. It is important to emphasize that the image quality changes observed in light and hard tapping were reversible, and because of the relative hardness of the bacterial spore coat, no structural damage occurred.

A major technical challenge to high-resolution AFM imaging is caused by variation in tip properties.[22,48–50] Double or multiple tip images of the same feature can be produced with an AFM probe having two or more endpoints that contact the surface simultaneously. Additionally, soft tapping imaging with a dull probe often results in poor quality or artefactual images with surface features (multiple bumps seen in Figure 2d) that reflect the shape of the tip, or the debris attached to it, rather than the true structure of the imaged spore surface.

Finally, for spores of species that possess exosporia (e.g., *B. cereus, B. thuringiensis*), these outer layers must be removed in order to visualize the underlying spore coat ultrastructure.[31,32] While the exosporium is of structural interest,[51,52] its outside layer is not as well ordered as the underlying coat layers.[31,32]

The high-resolution outer coat surface structure of air-dried spores. As seen in Figures 1c and 3, rodlet structures that form the surface layer of air-dried spores were covered with either individual loose rodlets or their networks, with considerable variation in the coverage density (Figure 3). Occasionally, these "surface" rodlets appeared to originate from the underlying rodlet layer. It is possible that these stray rodlets emerged as a result of spore dehydration and corresponding shrinkage of the outer coat. However, since networks of loose rodlets were also seen on substrate surfaces (data not shown), it is likely that in most cases these stray surface rodlets deposited from bulk solution during sample drying.

Stray rodlet networks were strongly attached to the outer spore coat surface and attached rodlets could not be displaced even during hard tapping (Figure 4a). Displacement could only be accomplished by AFM imaging of the spore surface in contact mode operation. In contact mode,[6,43] the probe remains in contact with the sample at all times during scanning, generating considerable lateral force. In this case, the lateral forces exerted were sufficient to 'sweep' networks of attached rodlets from the spore surface (Figure 4b).

Since one of the major functions of the spore coat is to protect the spore interior,[53,54] it is not surprising that the rodlet layer is rigid and unaffected by imaging in contact mode. However, when high forces were applied to a spore surface region, while imaging in contact mode, the ~11 nm thick layer of the rodlet structure was removed revealing the surface of the underlying integument (Figure 4c).

High-resolution surface structure of the hydrated spore coat. High-resolution rodlet structural images from fully hydrated spores are presented in Figure 5b,c. Very little is

known about the assembly, physical properties and proteomic nature of these bacterial spore rodlets. In the case of fungi, the rodlet layers of *Trichophyton mentagropytes* microconidia[55] and *Neurospora crassa* macroconidia[56] were found to be resistant to treatment by detergents, organic solvents, enzymes, alkali and mild acids, as is the bacterial spore coat.[44,54] Targeted mutations that resulted in removal of the rodlet layer from several fungal spore types produced a hydrophilic phenotype[57] which prevented the aerial dispersal of these spores. Hydrophobins, a new class of structural proteins,[58] were shown to be necessary for and an integral component of rodlet fungal spore surface structures. Hydrophobins can self-assemble and produce layers of rodlet structures at water-air interfaces.[58] However, while hydrophobin-like proteins are found in fungal spores, it has not been possible to identify orthologs of these proteins in bacterial spores (Leighton, T., unpublished). These similarities in crystalline outer coat layer motifs found in prokaryotic and eukaryotic spore types are a striking and unexpected example of the convergent evolution of critical biological structures. Further investigation is required to determine the molecular composition of prokaryotic endospore rodlets and their evolutionary relationship to eukaryotic rodlet structures.

Assembly of the spore coat rodlet structure. Biochemical and genetic studies have allowed considerable progress in defining spore coat assembly pathways and the function of morphogenetic proteins. A review of current status in the understanding of spore coat assembly is presented elsewhere.[44,54] While the self-assembly of the crystalline rodlet layer is one element among a complex process of spore coat morphogenesis, the existence and significance of this structure was not predicted by existing models for spore surface assembly.

AFM analysis has revealed stacking faults (indicated with white arrows in Figures 5a,b and 6a–c), which typically extended along the entire length of the outer coat surface. The height of these stacking faults varied from 0.2–11 nm, which corresponds to the partial or full height of a rodlet. Formation of stacking faults on the surfaces of inorganic, organic and protein crystals during their self-assembly is a well-known phenomena.[17,18,59,60] Stacking faults can occur due to the misfit of merging layers of a new structure during their nucleation and propagation. When imaging was performed using high force (Figure 6d), the partial removal of a rodlet layer revealed another layer of underlying rodlet structure (indicated with an arrow). The height of the upper rodlet layer was determined to be equal to 11 nm, consistent with the estimate of the thickness of the rodlet layer from EM analysis[1] and the measurement of rodlet width described here.

The surface layer of the outer spore coat of *B. atrophaeus* is typically formed by a single rodlet structural domain (Figure 7a). Multiple rodlet domains are less common (Figure 7b). In contrast to the single domain rodlet structure of the *B. atrophaeus* spore coat, multi-domain rodlet layers resembling a quilt,[31,32] were observed, as illustrated in Figure 7c, on the outer spore coat of *B. cereus* spores. In case of *B. thuringiensis* spores, rodlet structures were not observed as an integral component of the spore coat;[31,32] however, as illustrated in Figure 7d, patches of extrasporal rodlet structures were observed adsorbed to the substrate.[31,32]

Since AFM is a surface imaging technique, we cannot directly visualize the rodlet layer self-assembly process *inside* the sporulating cell. However, a model for spore

surface assembly, based on experimentally observed rodlet structural properties, can be derived from well-developed molecular-scale crystallization/self-assembly mechanisms.

The creation of the entire rodlet layer on the outer spore surface initiates with the nucleation/formation of a micro cluster (known in the crystallization and self-assembly literature as a critical nucleus) (Figure 8a1). Nucleation is a requirement for a first order phase transition, here the transition of rodlet-forming macromolecules from liquid into solid (semi-crystalline) phase. Upon subsequent addition of molecules to the critical nucleus, the structure extends laterally in both directions (Figure 8a2) and forms a rodlet superstructure, which continues to grow with a tangential rate V_t (Figure 8a3). As illustrated in Figure 8a3,4, the further development of the rodlet superstructure proceeds by the formation and growth of nuclei producing new, adjacent rodlets. The newly formed rodlet patch continues to grow with a rate V_n in a direction normal to the growth of individual rodlets. Based on energetical considerations,[59] formation of a new nucleus is more favorable on the edge of an existing rodlet than on an arbitrary spore surface location. The model described above is similar to the recently reported mechanism for advancement of growth steps by one-dimensional nucleation on the surfaces of protein and virus crystals.[14,16–18]

The rate-limiting step for development of the rodlet superstructure is the formation of nuclei on new adjacent rodlets. In one extreme case, if this nucleation rate is ~0, then $V_t >> V_n$, and the entire rodlet structure develops by growth of a single rodlet. In this case, until further growth is inhibited by preexisting rodlet loci, the single rodlet will keep wrapping around the spore as illustrated in Figure 8b. In the opposite extreme case, when the nucleation rate is very high and $V_n >> V_t$, then the development of the rodlet

structure proceeds as illustrated in Figure 8c. In this case, after fast normal growth is halted by self-inhibition, slow growth in the tangential direction results in multiple stacking faults. AFM visualization of rodlet layers on several hundred *B. atrophaeus* spores does not reveal stacking faults with the orientation corresponding to $V_n >> V_t$ (Figure 8b) or self-inhibited structures associated with $V_t >> V_n$ (Figure 8c). This indicates that during the assembly of the rodlet superstructure, growth rates for individual rodlets V_t and nucleation of adjacent rodlets V_n are comparable, and that the development of the rodlet layer proceeds as illustrated in Figure 8d. A limited number of stacking faults form when the single domain rodlet layer has completely enclosed the spore, and the two fronts either approach each other at a small angle (Figure 8e,f) or no angle, but have uneven heights (perhaps due to the uneven spore surface topography), which prevents the formation of a flawless superstructure. This model and the two stacking fault motifs illustrated in Figure 8e,f correlate well with experimentally observed rodlet structures (Figures 5 and 7a–c). The angle at which two rodlet fronts meet depends on the nucleation location and orientation of the original rodlet nucleus. The orientation of rodlet growth fronts could significantly change at the spore poles due to locally increased curvature. Indeed, the angle at which rodlet fronts meet varies as indicated in Figure 7a,b from ~0^o to 90^o.

The regular crystalline structure formed during rodlet layer assembly in the model is idealized, and in nature deviations from this structure were observed. These structural variations could be caused by non-ideal conditions during self-assembly due to adventitious incorporation of exogenous molecules or misincorporation of spore structural components. For example, in Figure 5c a number of “point” defects (indicated

with arrows) within rodlet structures, similar to “point” defects described in inorganic and macromolecular crystals,[17,59,61] were observed. These defects could be caused by the termination of rodlet growth due to incorporation of impurities at the rodlet growth tip. Subsequent to rodlet growth termination, the remaining row can be filled by another nucleated rodlet, leaving a small defect at the position of the impurity.

When the height misfit between two fronts of merging rodlet structures is similar to the thickness of the rodlet layer, upon merger, one layer could continue to grow above the other layer as shown in the diagram in Figure 8e,f. As illustrated in Figure 6c, during the assembly of a rodlet structure by merger of two opposite fronts, this overlap of layers was observed, resulting in the formation of a double-layered region. While the outer layer of the spore coat is formed by a single rodlet layer structure, there can be zones where two layers are present (Figure 6d). These discontinuities may explain the variable thickness of bacterial spore outer layers observed by thin section EM analysis.[1,3]

B. atrophaeus spore rodlet structures typically form as a single domain which is illustrated in Figure 8a, suggesting that initial nucleation of the rodlet took place in only one location. Multiple site rodlet structure nucleations, with arbitrary surface orientation and growth, would result in the formation of a structure with high mosaicity, as was observed for the *B. cereus* spore coat rodlet superstructure (Figure 7c). Analogous to crystal growth, the number of new phase nuclei (crystalline rodlet structures) and their growth rate is dependent on thermodynamics, kinetics of phase transitions, and variations in chemical and physical environments.[59]

During the sporulation process, macromolecules could self-assemble and form rodlet structures not only from the inner spore coat, but also independently from bulk

media. Such extrasporal rodlet structures were found in preparations of *B. thuringiensis* spores, (Figure 7d). The deposition of rodlet networks onto the surface of *B. atrophaeus* spores during dehydration (Figure 2) also suggests the presence of extraneous rodlets in bulk media. The width and thickness of rodlets forming the outer spore coat of *B. atrophaeus* and *B. cereus* spores were found to be similar to those of extrasporal rodlets observed in *B. thuringiensis* spore preparations. This suggests that similar rodlet structural elements are present in these three species of *Bacillus* spores. The origin of these stray rodlets is unclear. They could be deposited onto the spore surface by adsorption from bulk media or the mother cell cytoplasm.

The studies described here indicate that the striking differences in native rodlet structures seen in *B. atrophaeus*, *B. cereus* and *B. thuringiensis* are a consequence of species-specific nucleation and crystallization mechanisms which regulate the assembly of the outer spore coat. The chemical environment present (i.e., concentration of spore coat proteins, morphogenetic factors, salts, pH, temperature, etc.) during spore integument formation, as well as kinetic and thermodynamic parameters which control the formation of a new crystalline phase (i.e., surface free energy of formation of nucleus of a new phase), determine the macromolecular arrangement, structural association and topology of rodlet structures. Sporulation media compositions have the potential to alter considerably the structure of spore coat structural layers, which could affect spore functional properties. It is possible that under different sporulation conditions, rodlets could nucleate, assemble and attach to the outer coat of *B. thuringiensis* spores instead of being present in bulk media, as described above. One example of how solution chemistry during the sporulation process affects the formation of spore coat layers has been

reported.[1] The addition of Na_2SO_3 during sporulation of *B. cereus* resulted in the formation of longer rodlets within the domains of the cross patched rodlet layer. This result suggests that according to the model illustrated in Figure 8, addition of Na_2SO_3 caused a significant decrease in the rate of formation of new 1D nuclei.

These results demonstrate that concepts developed from studies of the nucleation and growth of inorganic and protein crystals[14,17,18,61] can be applied successfully to understanding the self-assembly of the outer endospore surface layer.

Acknowledgements

We thank A. McPherson for the use of the scanning probe microscope facilities in his laboratory at the University of California, Irvine, and S. Velsko and J. J. DeYoreo for helpful discussions and encouragement. This work was performed under the auspices of the U.S. Department of Energy by the University of California, Lawrence Livermore National Laboratory under Contract W-7405-Eng-48 and with support from the Defense Advanced Research Projects Agency.

References

(1) Aronson, A. I.; Fitz-James, P. *Bacteriol. Rev.* **1976,** *40***,** 360-402.

(2) Holt, S. C.; Leadbetter, E. R. *Bacteriol. Rev.* **1969**, *33*, 346-378.

(3) Wehrli, E.; Scherrer, P.; Kubler, O. *Eur. J. Cell. Biol.* **1980**, *20*, 283-289.

(4) Baker, T. S.; Olson, N. H.; Fuller, S. D. *Microbol. Mol. Biol. Rev*. **1999**, *63*, 862-922.

(5) Dubochet, J.; Adrian, M.; Richter, K.; Garces, J.; Wittek, R. *J. Virol.* **1994**, *68*, 1935-1941.

(6) Binnig, G.; Quate, C. F.; Gerber, C. *Phys. Rev. Lett.* **1986**, *56*, 930-933.

(7) Hoh, J. H.; Lal, R.; John, S. A.; Revel, J. P.; Arnsdorf, M. F. *Science* **1991**, *253*, 1405-1408.

(8) Karrasch, S. R.; Hegerl, R.; Hoh, J.H.; Baumeister, W.; Engel, A. *Proc. Nat. Acad. Sci. USA* **1994**, *91*, 836-838.

(9) Muller, D. J.; Engel, A. *J. Mol. Biol.* **1999**, *285*, 1347-1351.

(10) Schabert, F. A.; Henn, C.; Engel, A. *Science* **1995**, *268*, 92-94.

(11) Bustamante, C.; Rivetti, C. *Annu. Rev. Biophys. Biomol. Struct.***1996**, *25*, 395-429.

(12) Bustamante, C.; Rivetti, C.; Keller, D. J. *Curr. Opin. Sruct. Biol* **1997**, *7*, 709-716.

(13) Lyubchenko,Y. L.; Shlyakhtenko, L. S. *Proc. Natl. Acad. Sci. USA* **1997**, *94*, 496-501**.**

(14) Chernov, A. A.; Rashkovich, L. N.; Yaminski, I. V.; Gvozdev, N. V. *J. Phys.: Condens. Matter* **1999**, *11*, 9969-9984.

(15) Malkin, A. J.; Kuznetsov, Yu. G.; Land, T. A.; DeYoreo, J. J.; McPherson, A. *Nat. Struct. Biol.* **1995**, *2*, 956-959.

(16) Malkin, A. J.; McPherson, A. *J. Phys. Chem. B* **2002**, *106*, 6718-6722**.**

(17) Malkin, A. J.; Thorne, R. E. In *Methods: A Companion to Methods in Enzymology. Macromolecular Crystallization*; A. McPherson, Ed.; Elsevier Inc.: San Diego, 2004; Vol. 34/3, pp. 273-299.

(18) Vekilov, P. G.; Chernov, A. A. In *Solid State Physics*; Ehrenreich, H., Spaepen, F., Eds.; Academic Press: New York, 2002; Vol. 5, pp. 1-147.

(19) Kuznetsov, Yu. G.; Malkin, A. J.; Lucas, R. W.; Plomp, M.; McPherson, A. *J. Gen. Virol.* **2001**, *82*, 2025-2034.

(20) Kuznetsov, Yu. G.; Victoria, J. G.; Robinson, W. E., Jr.; McPherson, A. *J. Virol.* **2003**, *77*, 11896-11909.

(21) Malkin, A. J.; McPherson, A.; Gershon, P. D. *J. Virol.* **2003**, *77*, 6332-6340.

(22) Malkin, A. J.; Plomp, M.; McPherson, A. In *DNA Viruses: Methods and Protocols*; Lieberman, P. M., Ed.; Humana Press: Totowa, New Jersey, 2004; pp. 85-108.

(23) Plomp, M.; Rice, M. K.; Wagner, E. K.; McPherson, A.; Malkin, A. J. *Am. J. Pathol.* **2002**, *160*, 1959-1966.

(24) Camesano, T. A.; Natan, M. J.; Logan, B. E. *Langmuir* **2000**, *16*, 4563-4572.

(25) Sokolov, I. Yu.; Firtel, M.; Henderson, G. S. *J. Vac. Sci. Technol. A* **1996**, *14*, 674-678.

(26) Dufrêne Y. F. *Nat. Rev. Microbiol.* **2004**, *2*, 451-460.

(27) Dufrêne, Y. F.; Boonaert, C. J. P.; Gerin, P. A.; Asther, M.; Rouxhet, P. G. *J. Bacteriol.* **1999**, *181*, 5350-5354.

(28) Bowen, W. R.; Fenton, A. S.; Lovitt, R. W.; Wright, C. J. *Biotechnol. Bioeng.* **2002**, *79*, 170-179.

(29) Cross, J. B.; Currier, R. P.; Torraco, D. J.; Vanderberg, L. A.; Wagner, G. L.; Gladen, P. D. *Appl. Environ. Microbiol.* **2003**, *69*, 2245-2252.

(30) Chada, V. G. R.; Sanstad, E. A.; Wang, R.; Driks, A. *J. Bacteriol.* **2003**, *185*, 6255-6261.

(31) Plomp, M.; Leighton, T. J.; Wheeler, K. E.; Malkin, A. J. *Biophys. J.* **2005**, *88*, 603-608.

(32) Plomp, M.; Leighton, T. J.; Wheeler, K. E.; Malkin, A. J. *Langmuir* **2005**, accepted for publication.

(33) Fritze, D.; Pukall, R. *Int. J. Syst. Evol. Microbiol.* **2001**, *51*, 35-37.

(34) Penna T. C.; Marques, M.; Machoshvili, I. A.; Ishii, M. *Appl. Biochem. Biotechnol.* **2002**, *98*, 539-551.

(35) Young S. B.; Setlow, P. *J. Appl. Microbiol.* **2004**, *96*, 289-301.

(36) Burke, S. A.; Wright, J. D.; Robinson, M. K.; Bronk, B. V; Warren, R. L. *Appl. Environ. Microbiol.* **2004**, *70*, 2786-2790.

(37) Fergenson D. P.; Pitesky, M. E.; Tobias, H. J. & 17 other authors *Anal. Chem.* **2004**, *76*, 373-378.

(38) Whiteaker, J. R.; Fenselau, C. C.; Fetterolf, D.; Steele, D.; Wilson, D. *Anal. Chem.* **2004**, *76*, 2836-2841.

(39) Hodgson C. J.; Perkins, J.; Labadz, J. C. *Lett. Appl. Microbiol.* **2003**, *36*, 362-371.

(40) Lazzarini, R. A.; Santangelo, E. *J. Bacteriol.* **1967**, *94*, 125-130.

(41) Longchamp, P.; Leighton, T. *Lett. Appl. Microbiol.* **2000**, *31*, 242-246.

(42) Nicholson, W. L.; Setlow, P. In *Molecular Biological Methods for Bacillus*; Harwood, C. R., Cutting, S. M., Eds.; John Wiley & Sons: Chichester, West Sussex (UK), 1990; pp. 391-450.

(43) Magonov, S. N. In *Encyclopedia of Analytical Chemistry*; Meyers, R. A., Ed.; John Wiley & Sons Ltd., 2004; pp. 1-59.

(44) Driks, A. *Proc. Natl. Acad. Sci. USA* **2003**, *100*, 3007-3009.

(45) Westphal, A. J.; Price, P. B.; Leighton, T. J.; Wheeler, K. E. *Proc. Natl. Acad. Sci. USA* **2003**, *100*, 3461-3466.

(46) Cleveland, J. P.; Anczykowski, B.; Schmid, A. E.; Elings, V. B. *Appl. Phys. Lett.* **1998**, *72*, 2613-2615.

(47) Kumaki, J.; Nishikawa, Y.; Hashimoto, T. *J. Am. Chem. Soc.* **1996**, *118*, 3321-3322.

(48) Allen, M. J.; Hud, N. V.; Balooch, M.; Tench, R. J.; Seikhaus, W. J.; Balhorn, R. *Ultramicroscopy* **1992**, *42*, 1095-1100.

(49) Griffith, J. E.; Grigg, D. A. *J. Appl. Phys.* **1993**, *74*, R83-R109.

(50) Velegol, S. B.; Pardi, S.; Li, X.; Velegol, D.; Logan, B. E. *Langmuir* **2003**, *19*, 851-857.

(51) Todd, S. J.; Moir, A. J.; Johnson, M. J.; Moir, A. *J. Bacteriol.* **2003**, *185*, 3373-3378.

(52) Charlton, S.; Moir, A. J.; Baillie, L.; Moir A. *J. Appl. Microbiol.* **1999**, *87*, 241-245.

(53) Driks, A. *Microbiol. Mol. Biol. Rev.* **1999**, *63*, 1-20.

(54) Driks, A. *Trends Microbiol.* **2002**, *10*, 251-254.

(55) Hashimoto, T.; Wu-Yuan, C. D.; Blumenthal, H. J. *J. Bacteriol.* **1976**, *127*, 1543-1549.

(56) Beever, R. E.; Redgwell, R. J.; Dempsey, G. P. *J. Bacteriol.***1979**, *140*, 1063-1070.

(57) Beever, R. E.; Dempsey, G. P. *Nature* **1978**, *272*, 608-610.

(58) Wessels, J. G. *Adv. Microb. Physiol.* **1997**, *38*, 1-45.

(59) Chernov, A. A. In *Modern Crystallography III. Crystal Growth*. Springer-Verlag: Berlin, 1984.

(60) Malkin, A. J.; McPherson, A. In *From Solid-liquid Interface to Nanostructure Engineering*; Lin, X. Y., DeYoreo, J. J., Eds.; Plenum/Kluwer Academic Publisher: New York, 2004; Vol. 2, pp. 201-238.

(61) McPherson, A. In *Crystallization of Biological Macromolecules*; Cold Spring Harbor Laboratory Press: Cold Spring Harbor, 1999.

Figure legends

Figure 1. (a–c) AFM images of air-dried *B. atrophaeus* spores. Surface ridges, extending along the entire length of spores are indicated with arrows in (b). A surface area with a pronounced rodlet structure is indicated with arrows in (c). Scan areas and image types are: (a) 10 x 10 μm amplitude image; (b) 3.4 x 3.4 μm height image, and (c) 1.4 x 1.4 μm amplitude image.

Figure 2. (a–c) 0.4 x 0.4 μm AFM phase images of the same area studied with a dull AFM probe. (a) With moderate tapping conditions (A_{sp}/A_0 = 0.7) no surface features were seen; (b) harder tapping (A_{sp}/A_0 =0.4) resulted in the appearance of areas where high-resolution rodlet structure became visible; (c) Hard tapping (A_{sp}/A_0 =0.2) resulted in visualization of the rodlet layer (indicated with a black arrow). One of the individual stray rodlets is indicated with a white arrow. (d) A 750 x 750 nm amplitude image showing artifacts (numerous bumps on the spore coat surface) due to imaging with a contaminated, dull AFM probe.

Figure 3. High-resolution AFM phase images showing the regular rodlet structure of the outer coat of dried spores, which was covered with a network of stray rodlets. Scan areas are 530 x 530 nm (a) and 650 x 650 nm (b).

Figure 4. (a) A composite AFM tapping amplitude image showing the spore coat rodlet structure covered with stray rodlets. (b) Tapping amplitude image of the same area, visualized *after* scanning in AFM contact-mode. The network of stray rodlets has been

removed due to high contact-mode lateral forces, and the highly ordered rodlet structure of the outer spore coat is revealed. (c) Phase image showing that subsequent excessive force contact mode scanning of the area indicated by the accolade resulted in removal of the rodlet layer and visualization of the underlying integument.

Figure 5. AFM amplitude images of fully hydrated spores in water. Stacking faults on the rodlet layer of the spore coat are indicated with white arrows in (a,b). Surface wrinkles of the spore coat are indicated with black arrows (a). In (c), various "point defects" (indicated with black arrows) are seen in the high-resolution images of the rodlet structure. Scan areas are: (a) 1.9 x 1.9 μm; (b) 400 x 400 nm and (c) 120 x 120 nm.

Figure 6. (a–d) AFM images showing formation of rodlet structure stacking faults (indicated with arrows) by merger of opposite rodlet fronts at various angles. (a) 0^{o}; (b) ~90^{o}. In (c) an area where two rodlet fronts form a tile pattern (arrow) as described in Figure 8e. In (d) an area with a second layer of rodlet structure (indicated with an arrow) is exposed beneath the partially removed upper rodlet layer. Scan areas and image types are: (a) 500 x 500 nm height image; (b) 680 x 680 nm amplitude image; (c) 450 x 450 nm height image, and (d) 400 x 400 nm amplitude image.

Figure 7. (a) A typical single domain *B. atrophaeus* rodlet spore coat superstructure. In rare cases (b) three rodlets domains (indicated with 1, 2, 3) are observed. (c) Multi-domain crystalline rodlet structures of *B. cereus* spore surfaces. (d) Extrinsic rodlet assemblies can be seen adsorbed to the substrate of a *B. thuringiensis* spore preparation. These spores do not posses integral rodlet structures. Scan areas and image types are: (a)

500 x 500 nm phase image; (b) 650 x 650 nm amplitude image; (c) 370 x 370 nm phase image and (d) 800 x 800 nm amplitude image. Figures 7 c,d adapted from.[32]

Figure 8. Model for crystallization of the *B. atrophaeus* rodlet layer by a one-dimensional (1D) nucleation mechanism. Once a nucleus for a new crystalline phase is formed (a1), it expands both by tangential growth of individual rodlets, with velocity V_t, and laterally by 1D nucleation of new rodlets with a normal velocity of V_n. (a2–a4). (b) If tangential growth of rodlets V_t is much larger than the rate of 1D rodlet nucleation V_n, one single rodlet would grow rapidly and eventually inhibit itself, thereby prohibiting the formation of an organized, closed-packed layer. (c) If V_n is much larger than V_t, multiple rings of short rodlets would surround the spore, and produce stacking faults, which were not observed experimentally. (d) Based on the observed rodlet structure, the two growth vectors for the major domain of *B. atrophaeus* spores must have similar growth rates. (e–f) Various stacking fault motifs are formed by the encounter of two opposite rodlet fronts. Cases are shown where one front overlaps the other (e–f, gray circles), both fronts terminate leaving interstitial space (e–f, white circles), and two fronts form a tile pattern (e, black circle). Cases where two fronts continue growth in either an upward or downward (f, black circle) direction have not been observed.

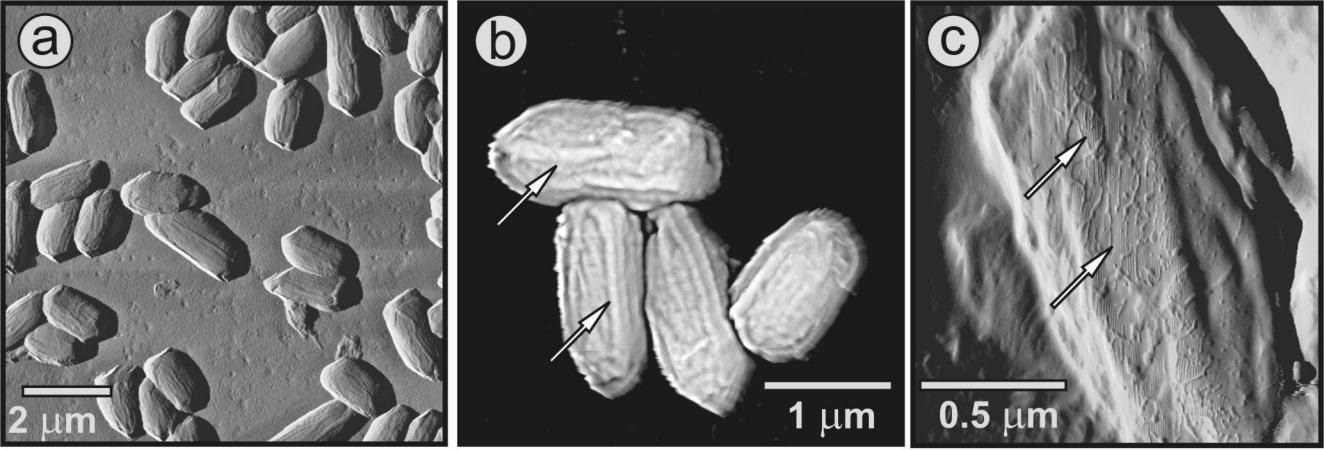

Figure 1

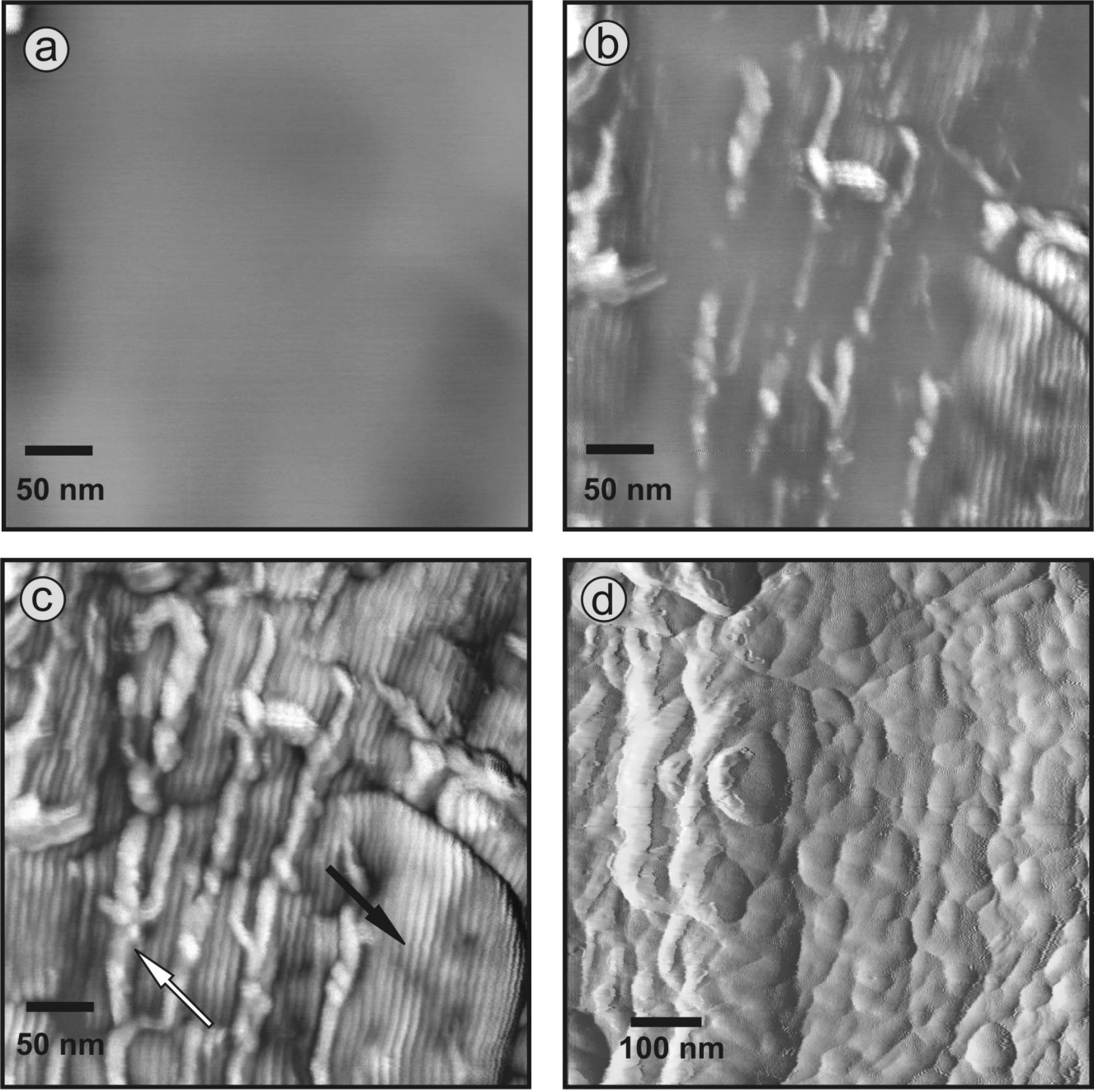

Figure 2

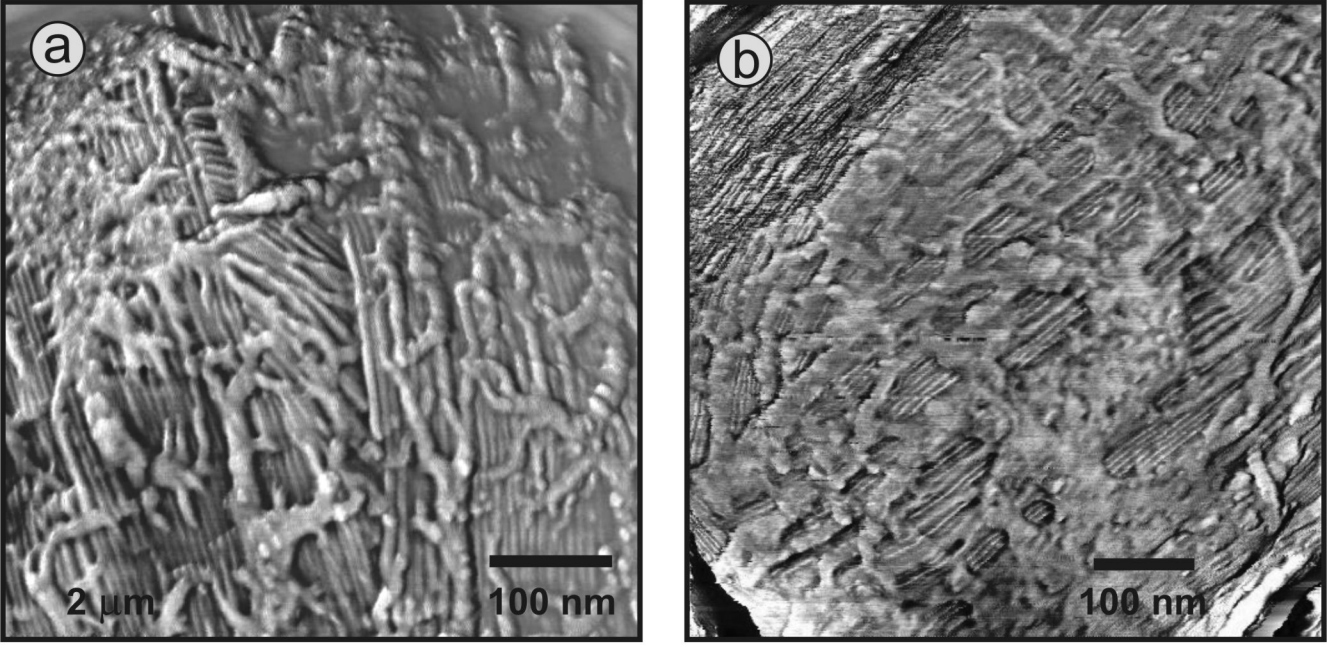

Figure 3

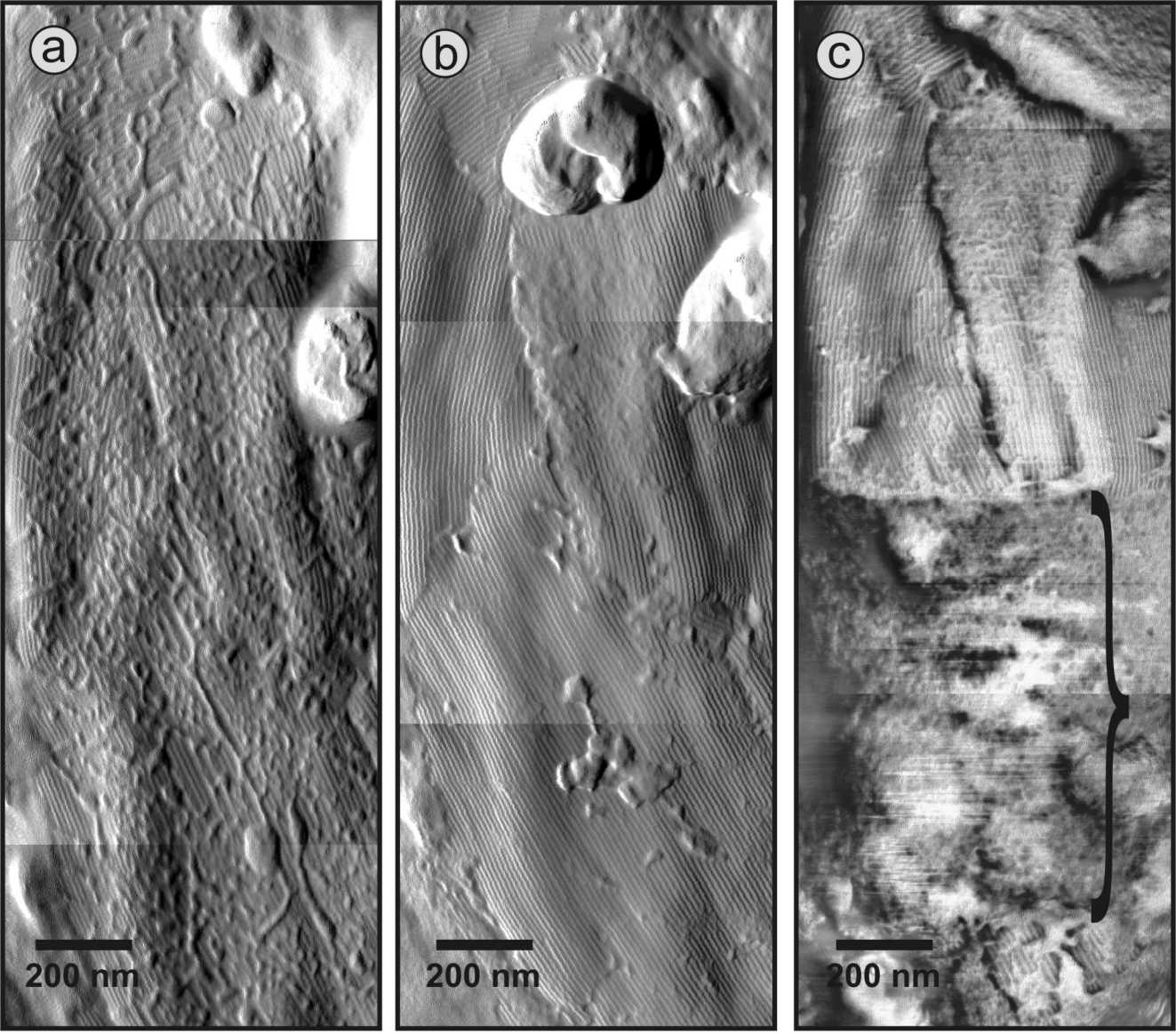

Figure 4

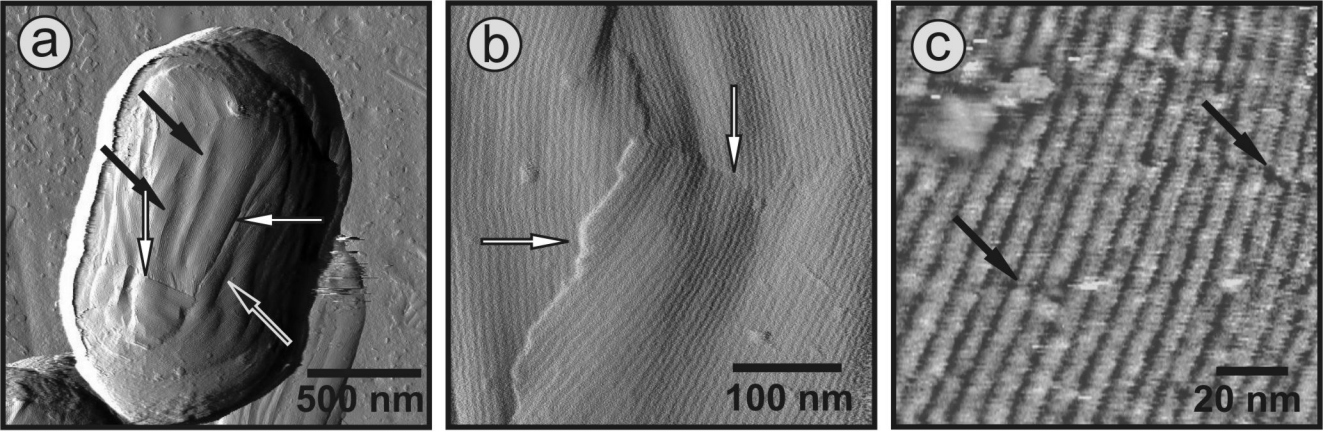

Figure 5

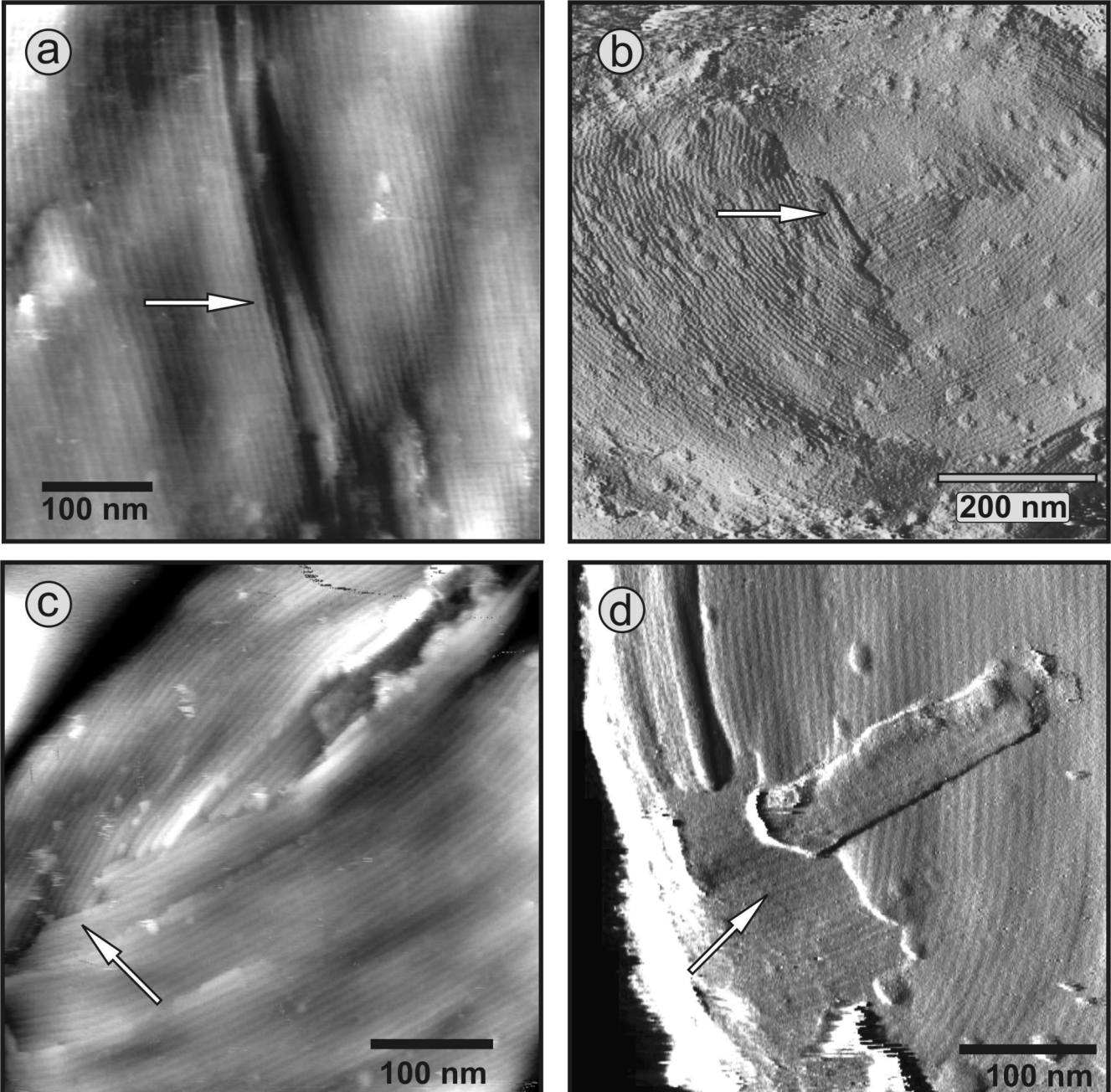

Figure 6

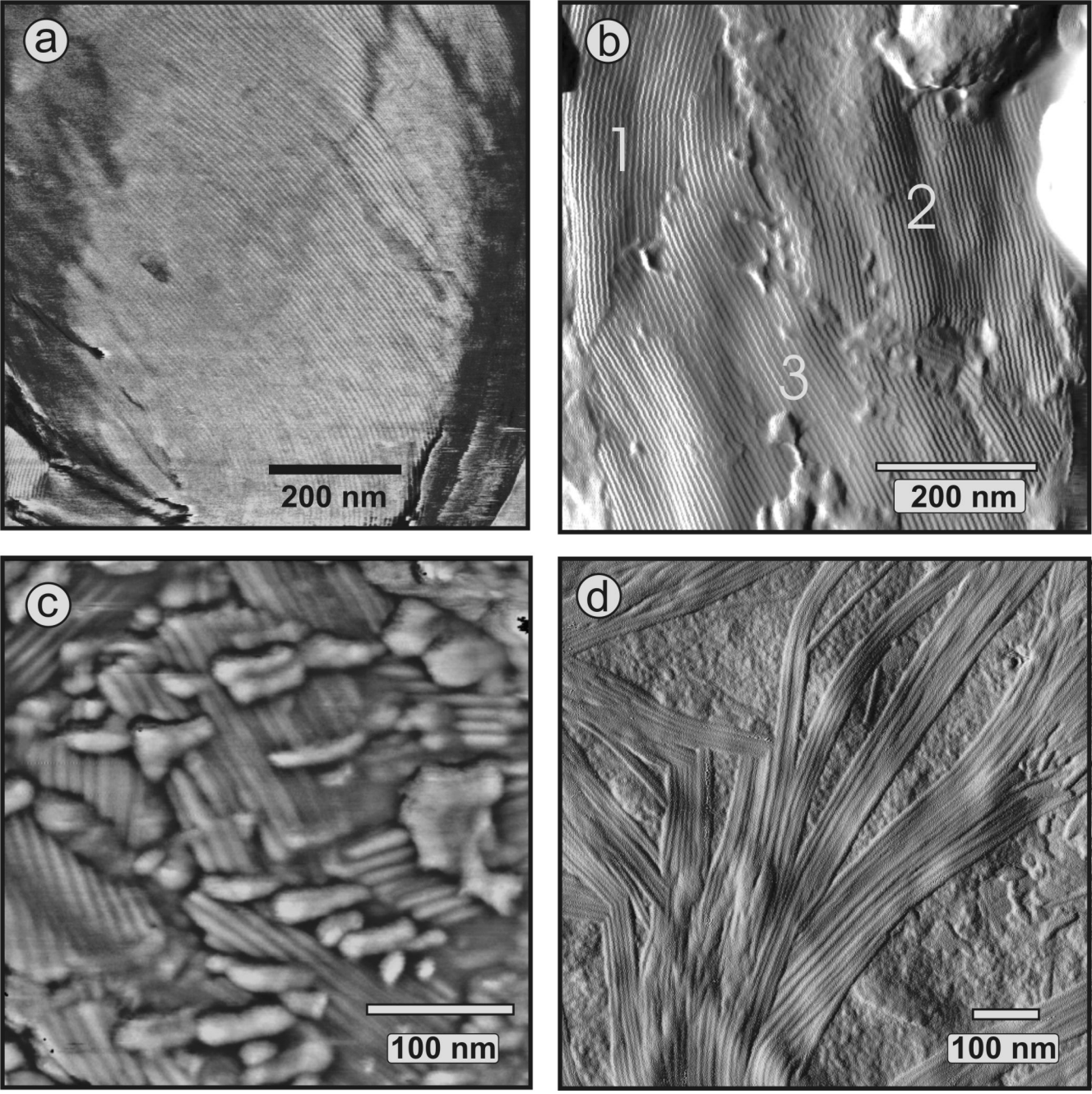

Figure 7

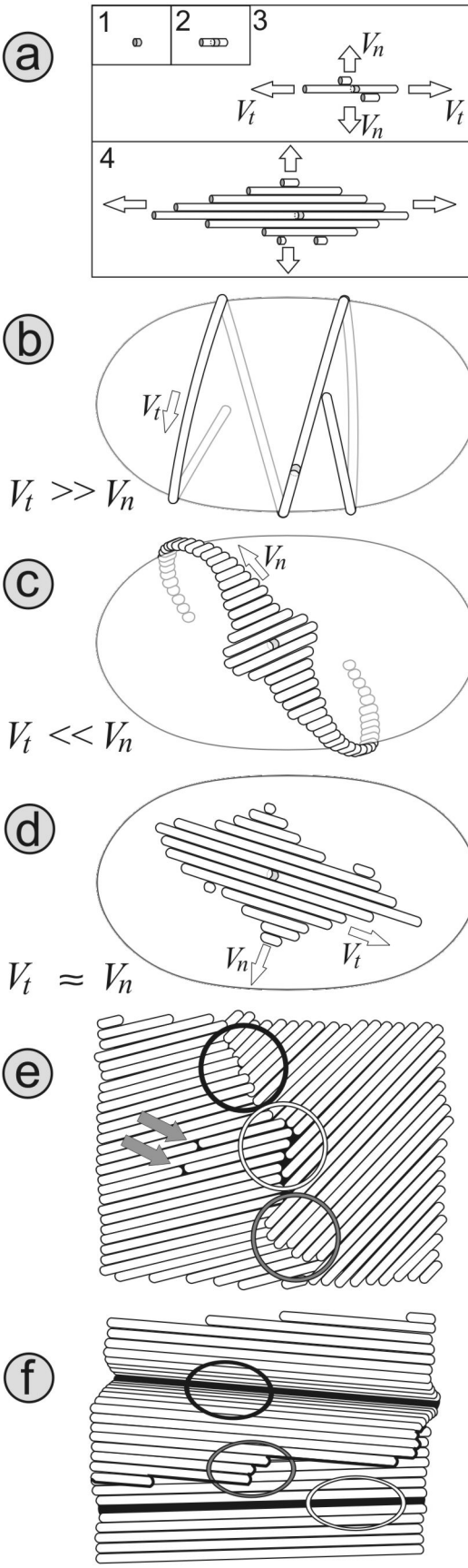

Figure 8